

Addendum: Action potential propagation and block in a model of atrial tissue with myocyte-fibroblast coupling

PETER MORTENSEN

*School of Mathematics & Statistics, University of Glasgow, Glasgow G12 8QQ
Institute of Cardiovascular & Medical Sciences, University of Glasgow, Glasgow G12 8TA*

HAO GAO

School of Mathematics & Statistics, University of Glasgow, Glasgow G12 8QQ

GODFREY SMITH

Institute of Cardiovascular & Medical Sciences, University of Glasgow, Glasgow G12 8TA

AND

RADOSTIN D. SIMITEV*

School of Mathematics & Statistics, University of Glasgow, Glasgow G12 8QQ

*Corresponding author. Email: Radostin.Simitev@glasgow.ac.uk

[Received on 23 February 2021; revised on 26 March 2021; accepted on 14 April 2021]

The analytical theory of our earlier study (Mortensen et al. (2021), *Mathematical Medicine and Biology*, 38(1), pp. 106-131) is extended to address the outstanding cases of fibroblast barrier distribution and myocyte strait distribution. In particular, closed-form approximations to the resting membrane potential and to the critical parameter values for propagation are derived for these two non-uniform fibroblast distributions and are in good agreement with numerical estimates.

Keywords: electrophysiology, myocyte—fibroblast coupling, refractoriness, asymptotic approximation

1. Introduction

The spatial distribution of fibroblasts within myocardial tissue, and the electrical coupling between fibroblasts and cardiomyocytes are significant but poorly-understood factors in triggering and sustaining cardiac arrhythmias. In our recent article (Mortensen et al., 2021) entitled “Action potential propagation and block in a model of atrial tissue with myocyte-fibroblast coupling”, hereinafter referred to as MGSS, we proposed that electrical propagation in fibrous tissue may be understood conceptually on the basis of three elementary fibroblast distributions: (C1) uniform, (C2) fibroblast barrier, and (C3) myocyte strait, illustrated in Fig. 1. Using direct numerical simulations, we then estimated primary action potential biomarkers including conduction velocity, peak potential and triangulation index and found that propagation block occurs at certain critical values of the parameters defining each of the elementary distributions. Based on a fast-slow scale analysis (Simitev & Biktashev, 2006; Biktashev et al., 2008; Simitev & Biktashev, 2011), we demonstrated that the boundary of absolute refractoriness in myocyte-fibroblast tissue is determined primarily by the value of the myocyte potential ahead of a propagating pulse and used this to obtain a simple analytic expression that captures with remarkable accuracy the block of propagation in the case of a uniform fibroblast distribution (C1).

The purpose of this addendum is to extend the analytical theory of MGSS to the remaining two ele-

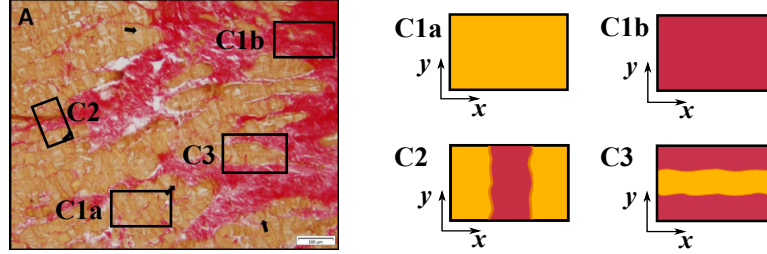


FIG. 1: A schematic illustration of fibroblast distributions C1 (uniform), C2 (fibroblast barrier) and C3 (myocyte strait) as they may appear in a border zone between intact myocardium and fibrosis. Red shades indicate high fibroblast density. To the left is an image of a border zone adapted by permission from BMJ Publishing Group (Yamamura et al., 2018). Propagation fronts are considered plane waves locally so coordinate systems are attached to the idealised regions only and propagation is along the x axis.

mentary fibroblast distribution cases – (C2) fibroblast barriers and (C3) myocyte straits. In the following, we derive and report closed-form approximations to the resting membrane potentials which allows us to estimate, also in closed-form, the critical parameter values separating electrical propagation from failure in these two non-uniform distributions. Our motivation for this analysis, the background literature on the topic and the notation used here are identical to those introduced in MGSS unless explicitly stated otherwise. Hence, we refer the reader to our earlier paper MGSS for these and further details.

2. Analytic approximations of propagation through fibroblast barriers and myocyte straits

Fibrous atrial tissue is modelled in MGSS as a 2D continuum of atrial myocytes where a fixed number of identical fibroblasts, $n(x, y)$, are connected in parallel at every Cartesian point (x, y) via an inter-cell conductance G_{gap} . In particular, the “fibroblast barrier” distribution (C2) is defined by

$$n(x, y) = NH(\Delta x/2 - x)H(x + \Delta x/2), \quad (2.1a)$$

and the “myocyte strait” distribution (C3) is defined by

$$n(x, y) = N \left(H(-y - \Delta y/2) + H(y - \Delta y/2) \right), \quad (2.1b)$$

and these are illustrated in Fig. 1. Here Δx and Δy are the widths of barriers and straits, respectively, N is a positive integer, and $H(\cdot)$ is the Heaviside step function. The propagation of electrical excitation in atrial tissues with such distributions is then described by a boundary value problem for the monodomain equations (2.1) of MGSS. Further, in MGSS we demonstrated that the boundary of absolute refractoriness is determined to a good approximation by the value of the myocyte potential ahead of a propagating pulse (prefront voltage), V_m^α . Note that, superscripts in V_m^α , and further below in V_m^0 , do not denote exponentiation.

We now consider action potentials travelling along the x axis in fully rested tissue with fibroblast distributions (2.1). Then, the prefront voltage V_m^α is identical to the steady state myocyte potential which we proceed to determine. Distributions (2.1) are functions of a single variable denoted by s for brevity, with s being x in the case of a fibroblast barrier and y in the case of a myocyte strait, respectively. Since

Case	Interval	K_1	K_2	K_3	λ
Fibroblast barrier (2.1a)	$s \in \left[0, \frac{\Delta s}{2}\right]$	$\frac{\sqrt{\kappa_1} \kappa_6}{2(\kappa_3 \kappa_7 + \kappa_8 \sqrt{\kappa_1})}$	$\frac{\sqrt{\kappa_1} \kappa_6}{2(\kappa_3 \kappa_7 + \kappa_8 \sqrt{\kappa_1})}$	$\frac{\kappa_4}{\kappa_3^2}$	$\kappa_3 \kappa_5$
	$s \in \left[\frac{\Delta s}{2}, \infty\right)$	$-\frac{\kappa_3 \kappa_6 \kappa_7}{\kappa_9(\kappa_3 \kappa_7 + \kappa_8 \sqrt{\kappa_1})}$	0	V_m^0	$\sqrt{\kappa_1} \kappa_5$
Myocyte strait (2.1b)	$s \in \left[0, \frac{\Delta s}{2}\right]$	$\frac{-\kappa_3 \kappa_6}{2(\kappa_3 \kappa_{11} + \kappa_{10} \sqrt{\kappa_1})}$	$\frac{-\kappa_3 \kappa_6}{2(\kappa_3 \kappa_{11} + \kappa_{10} \sqrt{\kappa_1})}$	V_m^0	$\sqrt{\kappa_1} \kappa_5$
	$s \in \left[\frac{\Delta s}{2}, \infty\right)$	$-\frac{\sqrt{\kappa_1} \kappa_6 \kappa_{10}}{\kappa_{12}(\kappa_3 \kappa_{11} + \kappa_{10} \sqrt{\kappa_1})}$	0	$\frac{\kappa_4}{\kappa_3^2}$	$\kappa_3 \kappa_5$

Table 1: Exponentials and constants of integration in the solution (2.3) of equations (2.2).

these functions are also even, the steady state version of equations (2.1) of MGSS can be reduced in both fibroblast distribution cases to a one-dimensional, time-independent system posed on the real half-line

$$\frac{d^2}{ds^2} V_m^\alpha = \frac{\chi}{\sigma_{ss}} (G_m(V_m^\alpha - V_m^0) + n(s)G_{\text{gap}}(V_m^\alpha - V_f^\alpha)), \quad s \in \mathbb{R}_+, \quad (2.2a)$$

$$0 = G_f(V_f^\alpha - V_f^0) + G_{\text{gap}}(V_f^\alpha - V_m^\alpha), \quad (2.2b)$$

$$\frac{d}{ds} V_m^\alpha(0) = 0, \quad \left[\frac{d}{ds} V_m^\alpha \right]_{s \rightarrow \infty} = 0. \quad (2.2c)$$

Here, χ is the cell surface-to-volume ratio, σ_{ss} with $s = x, y$ are the relevant diagonal component of the conductivity tensor and their values are listed in Table 1 of MGSS. To make the problem analytically tractable, we have also linearized the equations near the uncoupled resting potentials $V_m^0 = -81$ mV and $V_f^0 = -46$ mV of the original myocyte and fibroblast models of Courtemanche et al. (1998) and Morgan et al. (2016) as detailed in section 4.5 of MGSS, with G_m and G_f being the coefficients to the leading-order Taylor series terms. Equation (2.2b) is easily solved for the fibroblast resting potential V_f^α , and we are left with a boundary-value problem for a single second-order linear inhomogeneous ordinary differential equation for the myocyte resting potential V_m^α . Since the distributions $n(s)$ are piecewise constant, this resulting equation has constant coefficients in each of the intervals $s \in [0, \Delta s/2]$ and $s \in [\Delta s/2, \infty)$. Imposing continuity and smoothness matching conditions at $s = \Delta s/2$ and boundary conditions (2.2c), we find the solution

$$V_m^\alpha(s) = K_1 \exp(-\lambda s) + K_2 \exp(\lambda s) + K_3, \quad (2.3a)$$

$$V_f^\alpha(s) = (\kappa_2 V_m^\alpha(s) + V_f^0) / (\kappa_2 + 1). \quad (2.3b)$$

Here the constants K_1 , K_2 , K_3 and λ take different values in the intervals $s \in [0, \Delta s/2]$ and $s \in [\Delta s/2, \infty)$ and for the different choices of fibroblast distributions (2.1) as listed in Table 1 with further notation defined as

$$\kappa_1 = \frac{G_m}{G_{\text{gap}}}, \quad \kappa_2 = \frac{G_f}{G_{\text{gap}}}, \quad \kappa_3^2 = \frac{N\kappa_2 + \kappa_1 \kappa_2 + \kappa_1}{\kappa_2 + 1}, \quad \kappa_4 = \frac{N\kappa_2 V_f^0 + \kappa_1 V_m^0 (\kappa_2 + 1)}{\kappa_2 + 1}, \quad \kappa_5 = \sqrt{\frac{\chi G_{\text{gap}}}{\sigma_{ss}}},$$

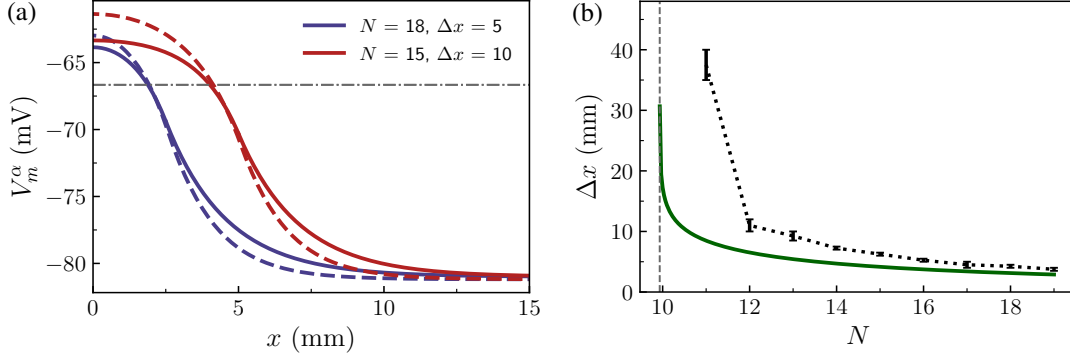


FIG. 2: Closed-form approximations in comparison to direct numerical simulations of MGSS for the case of fibroblast barrier distribution (2.1a). (a) Resting myocyte potential V_m^α . Expression (2.3) is shown by solid curves and numerical results are shown by broken curves both at values of N and Δx given in the legend. The thin dash-dotted line is the line $V_m^\alpha = E_h$. Propagation if successful is along the x axis. (b) Critical curve $\Delta x(N)$. Expression (2.7) is shown by a solid green curve and numerical results are shown by a dotted black curve with error bars. The numerical curve with error bars is the same one shown in Figure 6(a) of MGSS. The vertical asymptote N_{asy} is shown by thin dashed line.

$$\begin{aligned} \kappa_6 &= V_m^0 - \frac{\kappa_4}{\kappa_3^2}, \quad \kappa_7 = \sinh\left(\kappa_3 \kappa_5 \frac{\Delta s}{2}\right), \quad \kappa_8 = \cosh\left(\kappa_3 \kappa_5 \frac{\Delta s}{2}\right), \quad \kappa_9 = \exp\left(-\sqrt{\kappa_1} \kappa_5 \frac{\Delta s}{2}\right), \\ \kappa_{10} &= \sinh\left(\sqrt{\kappa_1} \kappa_5 \frac{\Delta s}{2}\right), \quad \kappa_{11} = \cosh\left(\sqrt{\kappa_1} \kappa_5 \frac{\Delta s}{2}\right), \quad \kappa_{12} = \exp\left(-\kappa_3 \kappa_5 \frac{\Delta s}{2}\right). \end{aligned} \quad (2.4)$$

The critical curves $\Delta s(N)$ partitioning the generic parameter planes $\pi(N, \Delta s)$ of the problem into regions of propagation and no-propagation are determined from the conditions

$$\max_{s \in [0, \infty)} V_m^\alpha(s) = E_h, \quad \text{and} \quad \min_{s \in [0, \infty)} V_m^\alpha(s) = E_h, \quad (2.5)$$

for fibroblast barrier and myocyte strait cases, respectively, as detailed in the formulation of equation (4.12) of MGSS. By the first of boundary conditions (2.2c), the profile $V_m^\alpha(s)$ has an absolute extremum at $s = 0$ equal to $V_m^\alpha(s = 0) = 2K_1 + K_3$. Hence, in the case of the fibroblast barrier distribution (2.1a), condition (2.5) becomes

$$\frac{\sqrt{\kappa_1} \kappa_6}{(\kappa_3 \kappa_7 + \kappa_8 \sqrt{\kappa_1})} + \frac{\kappa_4}{\kappa_3^2} = E_h. \quad (2.6)$$

This equation can be solved exactly for Δs . Indeed, the only terms that depend on Δs are κ_7 and κ_8 , and noting from (2.4) that $\kappa_7 = (\kappa_8^2 - 1)^{1/2}$, we solve the equation for κ_8 . Using the definition of κ_8 , we find a closed-form approximation for the critical curve in the case of the fibroblast barrier distribution (2.1a)

$$\Delta x = \frac{2}{\kappa_3 \kappa_5} \cosh^{-1} \left(\frac{\kappa_3 \sqrt{(E_h - \kappa_4/\kappa_3^2)^2 (\kappa_3^2 - \kappa_1) + \kappa_6^2 \kappa_1 + \kappa_6 \kappa_1}}{|E_h - \kappa_4/\kappa_3^2| (\kappa_3^2 - \kappa_1)} \right). \quad (2.7)$$

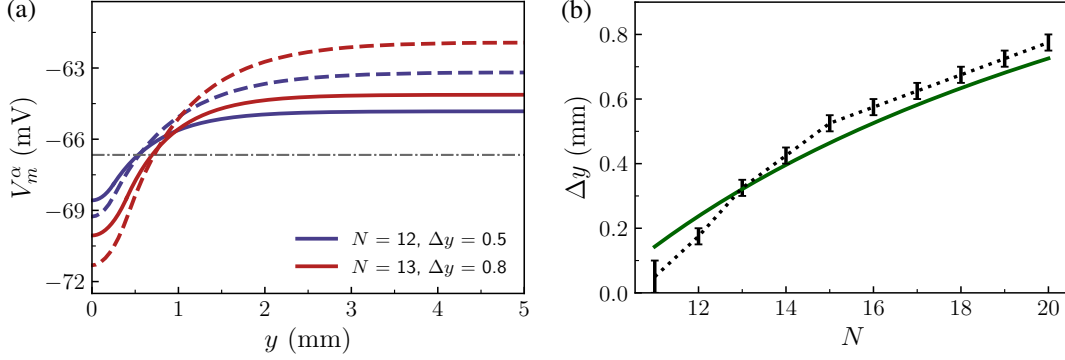


FIG. 3: Closed-form approximations in comparison to direct numerical simulations of MGSS for the case of myocyte strait distribution (2.1b). (a) Resting myocyte potential V_m^α . Expression (2.3) is shown by solid curves and numerical results are shown by broken curves both at values of N and Δy given in the legend. The thin dash-dotted line is the line $V_m^\alpha = E_h$. Propagation if successful is perpendicular to the y axis. (b) Critical curve $\Delta y(N)$. Expression (2.9) is shown by a solid green curve and numerical results are shown by a dotted black curve with error bars. The numerical curve with error bars is the same one shown in Figure 8(a) of MGSS.

Since K_1 does not vanish, we note that equation (2.6) cannot have any solutions precisely when $E_h = K_3$. The latter defines a vertical asymptote for the critical curve and can be solved explicitly to find

$$N_{\text{asy}} = \frac{\kappa_1(\kappa_2 + 1)(V_m^0 - E_h)}{\kappa_2(E_h - V_f^0)}. \quad (2.8)$$

This is in agreement with equation (4.12) of MGSS for the uniform distribution (C1) as the latter can be thought of as an infinitely wide fibroblast barrier.

For the myocyte strait distribution (2.1b) the approximation for the critical curve takes the form

$$\Delta s = \frac{2}{\sqrt{\kappa_1 \kappa_5}} \cosh^{-1} \left(\frac{\kappa_3^2 \kappa_6 + \sqrt{\kappa_1 (\kappa_3^2 \kappa_6^2 + (E_h - V_m^0)^2 (\kappa_1 - \kappa_3^2))}}{(E_h - V_m^0) (\kappa_1 - \kappa_3^2)} \right). \quad (2.9)$$

This is obtained from the condition $\min_{s \in [0, \infty)} V_m^\alpha(s) = 2K_1 + K_3 = E_h$ in a similar way to the fibroblast barrier case but rewriting first in terms of κ_{11} rather than κ_8 . This curve does not have a vertical asymptote as $V_m^0 \neq E_h$.

Figures 2 and 3 show a comparison of the derived closed-form approximations with values from the direct numerical simulations reported in MGSS for both fibroblast distributions. The discrepancy between the expression for the resting myocyte potential (2.3) and the numerical values is due to retaining only the linear terms in the Taylor expansions leading to the right-hand sides of the first two of equations (2.2). The expressions for the critical curves (2.7) and (2.9) are compared to the corresponding numerical curves shown in Figures 6(a) and 8(a) of MGSS, respectively, and their accuracy is additionally affected by the asymptotic reduction procedure used in MGSS to separate the description of fronts from the description of steady state equilibrium. However, the linearisation errors and the asymptotic

reduction errors seem to compensate each other resulting in a remarkably close agreement between the analytic and the numerical results for the critical curves of propagation. The direct numerical simulations of MGSS are, of course, also subject to numerical errors which are harder to estimate.

3. Conclusion

Two archetypal non-uniform spatial distributions of myocyte-fibroblast coupling were considered here. Approximations to the resting potentials of the coupled cells and to the distribution parameters at which action potential propagation is blocked were derived in explicit analytic form and are in good correspondence with values from direct numerical simulations. The results of the addendum are significant as they provide theoretical underpinning of realistic 2D and 3D computational studies where high fibroblast density as opposed to collagen accumulation leads to resting depolarization and spatial distribution of refractoriness (McDowell et al., 2011) and to the generation of complex fractionated atrial electrograms (Ashihara et al., 2012). Further, closed-form approximations of propagation in inhomogeneous medium such as the ones derived here can be used to estimate poorly constrained values of histological and electrophysiological parameters of myocardial tissue.

ACKNOWLEDGEMENTS This work was supported by the UK Engineering and Physical Sciences Research Council [grant numbers EP/N014642/1, EP/S030875/1 and EP/T017899/1].

References

- Ashihara, T., et al. (2012). The role of fibroblasts in complex fractionated electrograms during persistent/permanent atrial fibrillation. *Circ. Res.*, 110(2), 275–284, doi:[10.1161/circresaha.111.255026](https://doi.org/10.1161/circresaha.111.255026). 6
- Biktashev, V., et al. (2008). Asymptotic analysis and analytical solutions of a model of cardiac excitation. *Bull. Math. Biol.*, 70(2), 517–554, doi:[10.1007/s11538-007-9267-0](https://doi.org/10.1007/s11538-007-9267-0). 1
- Courtemanche, M., et al. (1998). Ionic mechanisms underlying human atrial action potential properties: insights from a mathematical model. *Am. J. Physiol.*, 275, H301–H321, doi:[10.1152/ajpheart.1998.275.1.h301](https://doi.org/10.1152/ajpheart.1998.275.1.h301). 3
- McDowell, K. S., et al. (2011). Susceptibility to arrhythmia in the infarcted heart depends on myofibroblast density. *Biophysical Journal*, 101(6), 1307–1315, doi:[10.1016/j.bpj.2011.08.009](https://doi.org/10.1016/j.bpj.2011.08.009). 6
- Morgan, R., et al. (2016). Slow conduction in the border zones of patchy fibrosis stabilizes the drivers for atrial fibrillation: insights from multi-scale human atrial modeling. *Frontiers in Physiology*, 7(474), doi:[10.3389/fphys.2016.00474](https://doi.org/10.3389/fphys.2016.00474). 3
- Mortensen, P., et al. (2021). Action potential propagation and block in a model of atrial tissue with myocyte–fibroblast coupling. *Math. Med. Biol.*, 38(1), 106–131, doi:[10.1093/imammb/dqaa014](https://doi.org/10.1093/imammb/dqaa014). 1
- Simitev, R. D. & Biktashev, V. (2006). Conditions for propagation and block of excitation in an asymptotic model of atrial tissue. *Biophys J*, 90, 2258–2269, doi:[10.1529/biophysj.105.072637](https://doi.org/10.1529/biophysj.105.072637). 1
- Simitev, R. D. & Biktashev, V. N. (2011). Asymptotics of conduction velocity restitution in models of electrical excitation in the heart. *Bul. Math. Biol.*, 73(1), 72–115, doi:[10.1007/s11538-010-9523-6](https://doi.org/10.1007/s11538-010-9523-6). 1
- Yamamura, K., et al. (2018). Electrotonic myofibroblast-to-myocyte coupling increases propensity to reentrant arrhythmias in two-dimensional cardiac monolayers. *Heart*, 108, 855–863, doi:[10.1136/heartjnl-2018-313961](https://doi.org/10.1136/heartjnl-2018-313961). 2